Optimal Kinematic Design of Spatial Parallel Manipulators: Application to Linear Delta Robot

Michael Stock*

Karol Miller
e-mail: kmiller@mech.uwa.edu.au

School of Mechanical Engineering,
The University of Western Australia,
Crawley/Perth WA 6009, Australia

An optimal kinematic design method suited for parallel manipulators is developed. The kinematic optimization process yields a design that delivers the best compromise between manipulability and a new performance index, space utilization. It is shown that the exhaustive search minimization algorithm is effective for as many as four independent design variables and presents a viable alternative to advanced nonlinear programming methods. The proposed kinematic optimization method is applied to the Linear Delta: a three degree of freedom translational manipulator. The kinematics of the Linear Delta are solved via the polynomial method. The mobility, workspace and manipulability characteristics are examined. It is shown that the Linear Delta's manipulability generally exhibits relatively little variation when compared to space utilization. The tendency exists for the solution to converge on a zero workspace size architecture when manipulability is optimized alone. The inclusion of the space utilization index in the cost function is crucial for obtaining realistic design candidates. [DOI: 10.1115/1.1563632]

1 Introduction

A parallel robot is one in which there exist two or more closed kinematic chains linking the base to the end effector. While the majority of robots in use today are serial in nature, parallel robots exhibit many favorable characteristics, such as high speeds and accelerations, low mobile masses, high stiffness, and superior accuracy. The most notable drawback of parallel robots is their relatively small workspaces.

The literature contains much information regarding the history and various types of parallel robots, e.g. [1–8]. Most important here, however, is the development of the DELTA by Clavel at the Institut de Microtechnique de l'Ecole Polytechnique Federale de Lausanne [1,2,9]. The DELTA consists of an equilateral triangle base, with one arm (actuated via a revolute joint) extending from each side of the base. The small, triangular traveling plate is connected to each arm via a pair of parallelogram forearms. The result is three translational degrees of freedom, with one additional uncoupled rotational degree of freedom at the end effector resulting from one further motor fixed to the base and connected to the end effector via a telescopic arm with two universal joints.

The Linear Delta, Fig. 1, is an adaptation of the DELTA, which results from replacing the revolute actuators and upper arms with three geometrically parallel linear actuators or rails. Furthermore, the fourth (rotational) degree of freedom is discarded. The literature to date lacks any detailed treatment of the Linear Delta.

The kinematics of the Linear Delta is simple, and is solved herein via direct manipulation of the three second order geometric constraint equations inherent in the structure. This approach is known in the literature as the Polynomial Method [4,10]. The inverse of the 3×3 Jacobian matrix, and hence the Jacobian itself, is determined by partial differentiation of the inverse kinematics equations with respect to the workspace coordinates.

While there exist several methods of determining the volume and boundaries of parallel manipulators' workspaces [1,11–13], the simplicity of the Linear Delta's geometry allows a relatively simple analysis to be carried out. Since the three linear actuators are geometrically parallel, the cross section of the workspace perpendicular to the actuators is constant (away from the practical limits of travel of the actuators), as are the Linear Delta's properties (such as manipulability) at any point in the cross section. For most practical Linear Delta structures, the cross sectional area and boundaries of the workspace may be found analytically. This phenomenon is exploited to greatly simplify the process of kinematic optimization.

In completing a kinematic optimization of the structure, four dimensionless design variables are chosen such that the results are applicable to any scale of Linear Delta. The optimization is carried out with the goal of reaching a compromise between two often-conflicting design goals: manipulability and workspace size. Maximization of the workspace volume alone tends to produce parallel or collinear joint axes (resulting in the manipulator being singular in all configurations), while considering manipulability in isolation may lead to architectures with relatively small workspaces; a clear example of this phenomena may be found in the results of [12]. Accordingly, the utility function considered here is a weighted sum of two performance indices.

The first index is based on that of [14], and measures the inverse of the Jacobian's condition number. This value is determined at many points, distributed evenly across the workspace cross section, and a sum (numerical integral) is taken. The result is normalized such that the index gives a measure of average manipulability over the cross section rather than a result dependent on total cross sectional area.

In order to overcome the limitations associated with the use of this index in isolation, a new performance index is proposed which measures *space utilization*, and reflects the ratio of the workspace size to the physical size of the robot's structure. The size of the robot is estimated by the area of the bounding box enclosing the robot's structure and workspace in the cross section. This index has been developed to penalize designs which are large and unwieldy yet produce small workspaces, such as those that result from optimizing manipulability alone.

2 Linear Delta Manipulator Description

The structural parameters of the Linear Delta, as shown in Figs. 2 and 3, may be summarized as:

*Presently at: Advanced Analysis Group-Worley Limited, Level 6, 250 St Georges Terrace, Perth WA 6000, Australia

Contributed by the Mechanisms Committee for publication in the JOURNAL OF MECHANICAL DESIGN. Manuscript received August 2001; rev. August 2002. Associate Editor: D. C. H. Yang.

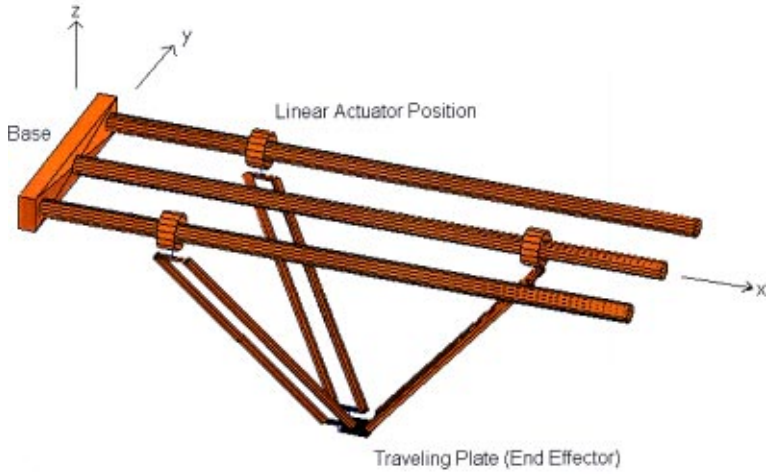

Fig. 1 Rendered MATLAB representation of the Linear Delta

L_1	Length of outer parallelogram arms one and three ($L_3=L_1$).
L_2	Length of central parallelogram arms.
$2\cdot Y_R$	Separation (y direction) of (outer) Rails One and Three.
Z_R	Separation (z direction) of Rails One and Two.
Y_A	Asymmetric offset of Rail Two (y direction).
$\mathbf{q}=(X_1,X_2,X_3)$	Joint space variables—displacements of actuators along the rails.
$\mathbf{x}=(x,y,z)$	Workspace variables—position of end effector in workspace coordinates.

2.1 Mobility. The ends of all arms are connected directly to either the travelling plate or the corresponding actuator by ball joints. There are twelve ball joints, three prismatic joints and eleven links, including the base. Applying the Grübler formula:

$$M=6(n-j-1)+\sum_{i=1}^{j} f_i \tag{1}$$

where n is the number of links (including the base), j is the number of joints and joint i $(1\leqslant i\leqslant j)$ has connectivity f_i, yields a mobility of nine. As suggested by Fig. 1, each arm's motion is restricted only by ball joints at both ends. Each arm is therefore free to rotate about the axis joining its endpoints, and six idle degrees of freedom exist within the mechanism. The true mobility of the mechanism (external degrees of freedom) is thus three.

2.2 Kinematics of Linear Delta

2.2.1 Constraint Equations. The constraint equations for the Linear Delta (2) are generated by applying Pythagoras' rule in three dimensions to each pair of arms. Noting that $L_1=L_3$, the equations define three spheres:

$$\begin{aligned}
&(a)\quad (x-X_1)^2+(y-Y_R)^2+z^2=L_1^2\\
&(b)\quad (x-X_2)^2+(y-Y_A)^2+(z-Z_R)^2=L_2^2\\
&(c)\quad (x-X_3)^2+(y+Y_R)^2+z^2=L_1^2
\end{aligned} \tag{2}$$

2.2.2 Inverse Kinematics. Consider one kinematic chain of the Linear Delta, consisting of the end effector, one pair of parallelogram arms, one actuator, and the base. For a given end effector position **x**, the location of the lower end of the arm pair is known. All possible positions of the upper end are then described by the surface of a sphere centered at the lower end with a radius equal to the arm length. The intersection of this sphere with the line of action of the actuator gives the possible actuator position(s). The geometry is further simplified by the line of action of each actuator being parallel to the x-axis.

The intersection of a line and a sphere generally has two solutions. Alternatively, if the line is tangent to the sphere, then there

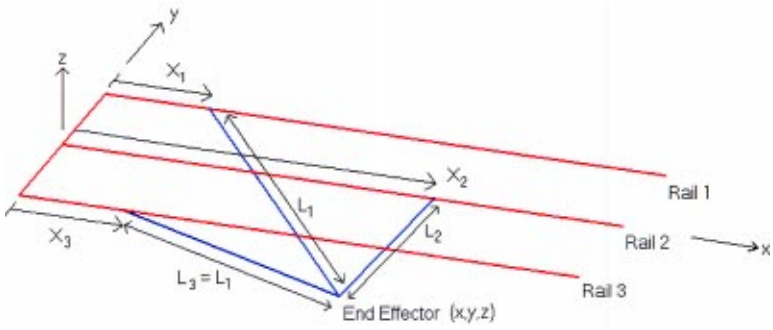

Fig. 2 Wireframe representation of Linear Delta showing nomenclature

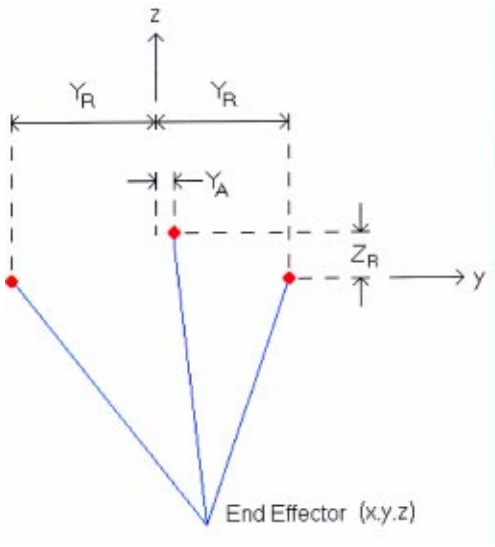

Fig. 3 End view (*y-z* plane) of wireframe representation showing nomenclature

exists only one solution—this corresponds to the physical situa tion whereby the end effector is lying on the workspace boundary. If the line does not intersect the sphere, then there is no solution, implying that the specified end effector position is outside of the robot's workspace.

The presence of three actuators, each with (generally) two possible positions, gives $2^3=8$ possible solutions to the inverse kinematics. Note that each pair of arms is considered as a single member here, as illustrated in Fig. 4.

The algorithm presented in (3) below yields the solution that maximizes X_2 and minimizes both X_1 and X_3, representing the robot the configuration show in the upper left boxed portion of Fig. 4.

$$
\begin{aligned}
&(a)\quad (x-X_1)^2+(y-Y_R)^2+z^2=L_1^2\\
&\qquad \Rightarrow X_1=x-\sqrt{L_1^2-z^2-(y-Y_R)^2}\\
&(b)\quad (x-X_2)^2+(y-Y_A)^2+(z-Z_R)^2=L_2^2\\
&\qquad \Rightarrow X_2=x+\sqrt{L_2^2-(z-Z_R)^2-(y-Y_A)^2}\\
&(c)\quad (x-X_3)^2+(y+Y_R)^2+z^2=L_1^2\\
&\qquad \Rightarrow X_3=x-\sqrt{L_1^2-z^2-(y+Y_R)^2}
\end{aligned}
\tag{3}
$$

2.2.3 Forward Kinematics For $Z_R\neq 0$. Solving the Forward Kinematics of the Linear Delta involves finding the intersection point of three spherical surfaces, illustrated in Fig. 5. The surface of each sphere represents the range of motion of the lower end of one of the arms when its upper end occupies a known position (determined from the geometry of the robot and the extension of the appropriate actuator). The radius of each sphere is equivalent

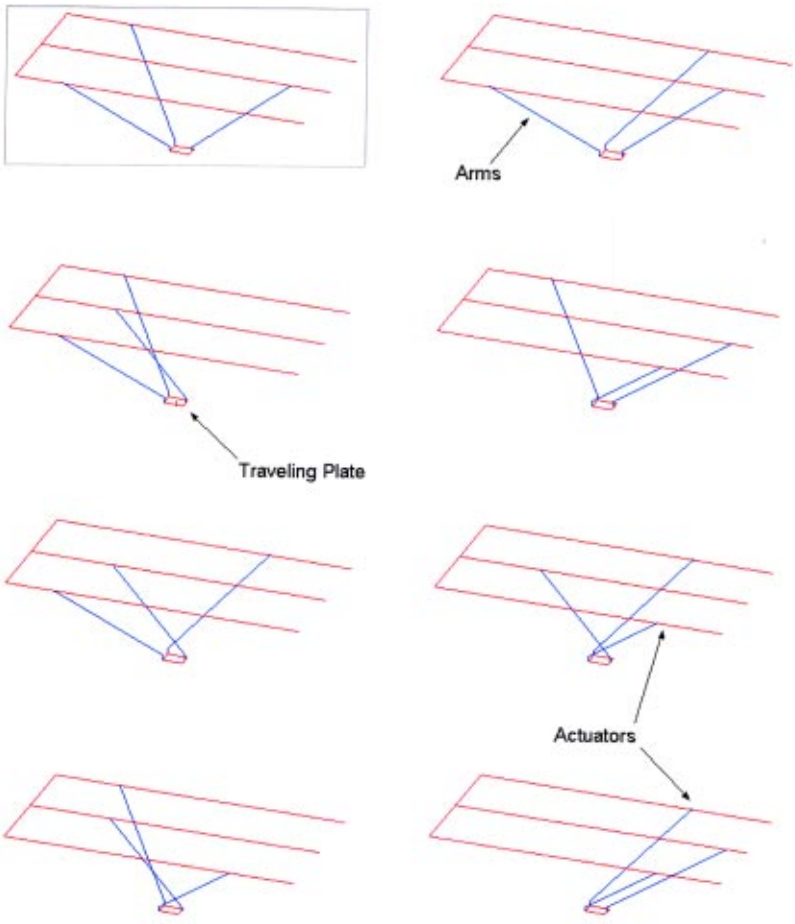

Fig. 4 Stick representation of the eight solutions for the inverse kinematics of the Linear Delta

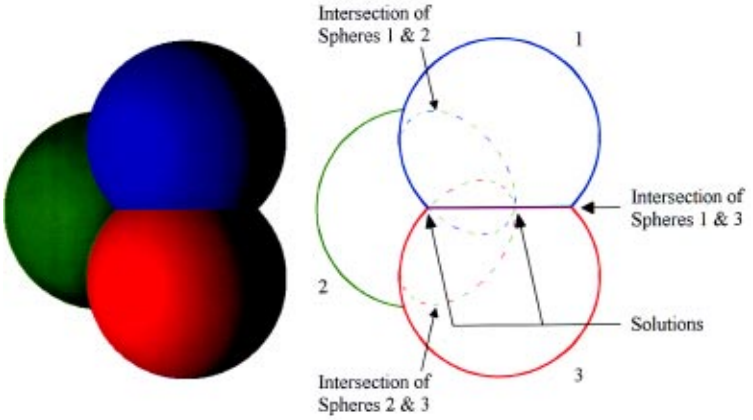

Fig. 5 Forward kinematics of the Linear Delta visualized as the intersection of three spheres

to the length of the corresponding arm, and the intersection point(s) of the three sphere surfaces is (are) the only possible position(s) that the end effector may occupy.

In the general case, there exist two intersection points. Other cases have been identified in [15], including a situation where infinite number of solutions exist when the centers of two or more spheres coincide. For the Linear Delta, however, there exist only three possibilities:

1. General solution—two intersection points exist.
2. Singular solution—one sphere is tangent to the circle of intersection of the two other spheres, resulting in one unique solution.
3. No solution—no intersection point exists.

It has been shown that solving for the intersection of three spheres may be completed in closed form [15]. Firstly, two of the constraint equations, (2*a*) and (2*c*), are expanded and rearranged:

$$y = x\left(\frac{X_3 - X_1}{2Y_R}\right) + \left(\frac{X_1^2 - X_3^2}{4Y_R}\right) = Ax + B \tag{4}$$

A and *B*, used here for simplicity (as with *C*, *D*, *E*, *F*, *G*, *H*, *I*, *K*, *L*, and *M* below), depend only on the geometry and actuator positions. A similar approach may be taken with constraints (2*b*) and (2*c*). When the expression for the *y* coordinate given in (4) is substituted into these equations, the result is an expression relating *x* and *z*, of the form:

$$z = x\left(\frac{X_3 - X_2 - A(Y_R + Y_A)}{Z_R}\right) + \left(\frac{-1}{2Z_R}\right)(Y_R^2 - X_2^2 + X_3^2 - L_1^2 + L_2^2 - Y_A^2 - Z_R^2 + 2B(Y_R + Y_A)) = Cx + D \tag{5}$$

Substituting (4) and (5) into (2*b*) yields a quadratic in *x*, of the form:

$$\begin{aligned} Ex^2 + Fx + G &= 0 \\ E &= 1 + A^2 + C^2 \\ F &= 2(AB + CD - X_2 - Y_A A - Z_R C) \\ G &= B^2 - 2Y_A B + D^2 + X_2^2 - L_2^2 + Y_A^2 + Z_R^2 - 2Z_R D \end{aligned} \tag{6}$$

The two solutions to the quadratic of (6) correspond to the two points at which the three spheres intersect. One such point is located below the actuators ($z<0$), and one above ($z>0$). In order to ensure the correct ($z<0$) solution is generated, the sign of Z_R must be considered:

$$x = \begin{cases} \dfrac{-F + \sqrt{F^2 - 4EG}}{2E} & \text{when } Z_R > 0 \\ \dfrac{-F - \sqrt{F^2 - 4EG}}{2E} & \text{when } Z_R < 0 \end{cases}$$

$$\begin{aligned} y &= Ax + B \\ z &= Cx + D - Z_{TP} \end{aligned} \tag{7}$$

2.2.4 Forward Kinematics for Coplanar Actuators ($Z_R=0$). The solution given in Section 2.2.3 fails when $Z_R=0$, due to vanishing denominators in (5). A similar solution procedure may, however, be adopted after substituting $Z_R=0$ into (2). Expanding and subtracting (2*a*) from (2*c*) yields:

$$x = y\left(\frac{2Y_R}{X_3 - X_1}\right) + \left(\frac{X_3 + X_1}{2}\right) = Hy + I \tag{8}$$

Similarly, expanding and subtracting (2*a*) from (2*b*) gives:

$$x = y\left(\frac{Y_R - Y_A}{X_2 - X_1}\right) + \left(\frac{L_2^2 - L_1^2 - Y_A^2 + Y_R^2 + X_1^2 - X_2^2}{2(X_1 - X_2)}\right) = Ky + M \tag{9}$$

Equating (8) and (9) yield *x* and *y*. Substitution into (2*a*) yields the *z* coordinate:

$$\begin{aligned} y &= \frac{1 - M}{K - H} \\ x &= Hy + I \\ z &= -\sqrt{L_1^2 - (x - X_1)^2 - (y - Y_R)^2} \end{aligned} \tag{10}$$

It should be noted that the denominator of (8) vanishes under the condition $X_1 = X_3$, in which case the following solution may be employed:

$$\begin{aligned} x &= M \\ y &= 0 \\ z &= -\sqrt{L_1^2 - (x - X_1)^2 - Y_R^2} \end{aligned} \tag{11}$$

The case of a vanishing denominator in (9) may be ignored, since the assumed posture of the robot (see Fig. 4) ensures that $X_2 > X_1$.

Finally, the Polynomial Method was compared to Newton's Iterative Method [4,10] in order to evaluate their respective com-

putational efficiencies. It was found that each iteration of Newton's Method was more expensive than the closed form implementation of the Polynomial Method.

2.3 The Jacobian Matrix of Linear Delta. The Inverse Kinematics relationships for the Linear Delta are relatively simple. Therefore, the most computationally efficient method of calculating the Jacobian Matrix is to differentiate these relationships with respect to x, y and z, yielding the elements of the Inverse Jacobian, and inverting this matrix.

The terms of J^{-1} may be calculated from partial derivatives of (3):

$$J^{-1}=\begin{bmatrix} 1 & \dfrac{y-Y_R}{\sqrt{L_1^2-z^2-(y-Y_R)^2}} & \dfrac{z}{\sqrt{L_1^2-z^2-(y-Y_R)^2}} \\ 1 & \dfrac{Y_A-y}{\sqrt{L_2^2-(z-Z_R)^2-(y-Y_A)^2}} & \dfrac{Z_R-z}{\sqrt{L_2^2-(z-Z_R)^2-(y-Y_A)^2}} \\ 1 & \dfrac{y+Y_R}{\sqrt{L_1^2-z^2-(y+Y_R)^2}} & \dfrac{z}{\sqrt{L_1^2-z^2-(y+Y_R)^2}} \end{bmatrix}=\begin{bmatrix} 1 & J_{12}^{-1} & J_{13}^{-1} \\ 1 & J_{22}^{-1} & J_{23}^{-1} \\ 1 & J_{32}^{-1} & J_{33}^{-1} \end{bmatrix} \tag{12}$$

The Jacobian is then obtained through the inversion of J^{-1}. A relatively simple closed form expression is possible since the inverse Jacobian is a 3×3 matrix:

$$J=\frac{1}{J_{22}^{-1}J_{33}^{-1}-J_{23}^{-1}J_{32}^{-1}-J_{12}^{-1}J_{33}^{-1}+J_{13}^{-1}J_{32}^{-1}+J_{12}^{-1}J_{23}^{-1}-J_{13}^{-1}J_{22}^{-1}}\begin{bmatrix} J_{22}^{-1}J_{33}^{-1}-J_{23}^{-1}J_{32}^{-1} & J_{13}^{-1}J_{32}^{-1}-J_{12}^{-1}J_{33}^{-1} & J_{12}^{-1}J_{23}^{-1}-J_{13}^{-1}J_{22}^{-1} \\ J_{23}^{-1}-J_{33}^{-1} & J_{33}^{-1}-J_{13}^{-1} & J_{13}^{-1}-J_{23}^{-1} \\ J_{32}^{-1}-J_{22}^{-1} & J_{12}^{-1}-J_{32}^{-1} & J_{22}^{-1}-J_{12}^{-1} \end{bmatrix} \tag{13}$$

Singularities occur within the workspaces of parallel manipulators where $\det(J^{-1})=0$. In these configurations, an external force may infinitesimally move the end effector while the actuators remain stationary, the actuator forces or torques required to move the end effector in certain directions tend to infinity, and the manipulator gains additional degrees of freedom [14,16].

Analysis of the Linear Delta's workspace reveals that there exists a singularity surface near the actuators. When $Z_R=0$, and the linear actuators are coplanar, it is simple to prove that this singularity surface is the plane $z=0$, since the third column of J^{-1} consists entirely of zeros in this case. The surface becomes more complex as Z_R is varied, however all points on the surface correspond to configurations in which the parallelogram arms are coplanar.

A degenerate singularity also occurs when $Y_R=0$, as rows one and three of J^{-1} become identical. Inverse singularities, where $\det(J)=0$, have not been considered here.

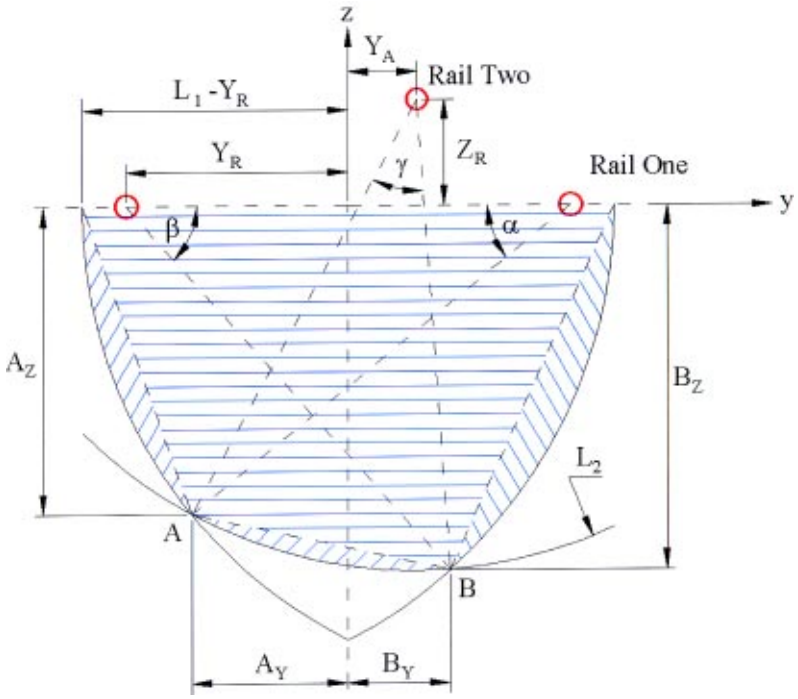

Fig. 6 Workspace cross section for case 1

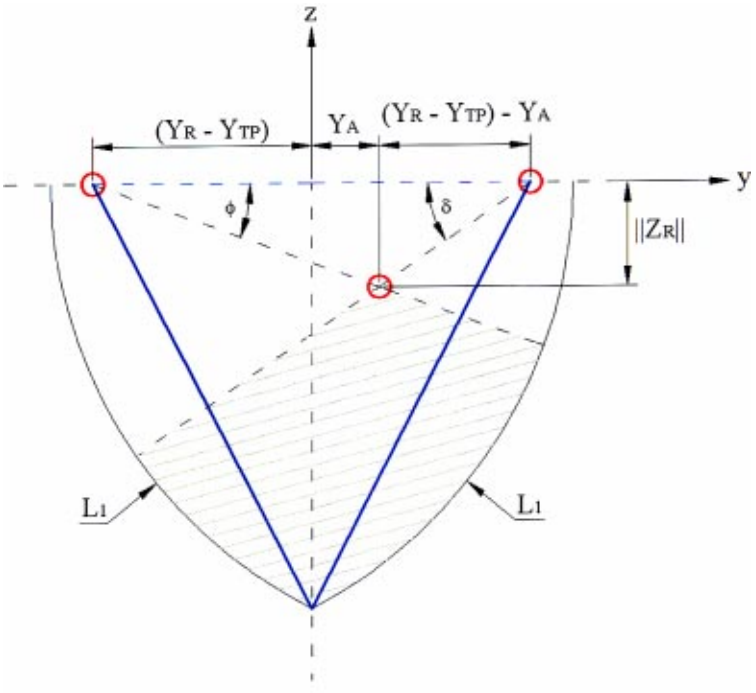

Fig. 7 Workspace cross section for case 2

2.4 Workspace Cross Section Analysis of Linear Delta. When considering regions away from the limits of travel of the actuators, the Linear Delta's cross section in the *y*-*z* plane is constant, with its boundaries defined by:

1. Three circles, each centered on one actuator's position, with a radius equal to the length of the corresponding parallelogram arms (L_1 or L_2).
2. The plane $z=0$, through which the end effector cannot pass.
3. If $Z_R<0$, the position of the central actuator restricts the inward motion of the outer arms.

In this analysis, the components are considered to occupy infinitesimally small volumes of space, all joints are assumed unrestricted in their motion, and clashing within the parallelogram structures is ignored. Two specific geometric cases are presented here, encompassing the vast majority of practical architectures of the Linear Delta—an exhaustive coverage of all possible structures would be prohibitively lengthy and tedious, with little practical use.

2.4.1 Case 1: $Z_R \geq 0$. Figure 6 illustrates this case, and defines the variables used below. The hatched area denotes the workspace cross section. Note that the length of the central parallelogram arms, L_2, is such that the arc transcribed by these arms forms part of the workspace cross section boundary; increasing L_2 until the intersection points *A* and *B* in Fig. 6 vanished would considerably simplify the analysis. The coordinates of points *A* and *B* may be determined by solving the following pairs of equations:

$$\begin{matrix} A & B \end{matrix}$$
$$\begin{bmatrix} (y-Y_A)^2+(z-Z_R)^2=L_2^2 \\ (y-Y_R)^2+z^2=L_1^2 \end{bmatrix} \quad \begin{bmatrix} (y-Y_A)^2+(z-Z_R)^2=L_2^2 \\ (y+Y_R)^2+z^2=L_1^2 \end{bmatrix} \tag{14}$$

A very simple closed form algorithm for solving systems of equations of this type can be obtained by hand, its derivation is omitted here for succinctness. This calculation of the coordinates of *A* and *B* in the *y*-*z* plane, denoted (A_y, A_z) and (B_y, B_z) respectively, allows the values of α, β and γ to be determined, which define the angles subtended by each segment (see Fig. 6):

$$\cos\alpha=\frac{Y_R+A_Y}{L_1} \quad \cos\beta=\frac{Y_R+B_y}{L_1}$$
$$\gamma=\arcsin\left[\frac{B_y-Y_A}{L_2}\right]+\arcsin\left[\frac{A_y+Y_A}{L_2}\right] \tag{15}$$

Finally, the cross sectional area may be calculated:

$$\text{Area}=\frac{1}{2}L_1^2(\alpha-\sin\alpha+\beta-\sin\beta)+\frac{1}{2}L_2^2(\gamma-\sin\gamma)+(A_y+B_y)$$
$$\times\left[\frac{A_z+B_z}{2}\right]+\frac{1}{2}A_z(L_1-Y_R-A_y)+\frac{1}{2}B_z(L_1-Y_R-B_y) \tag{16}$$

2.4.2 Case 2: $Z_R<0$. When Z_R assumes a negative value, the presence of the central rail further limits the workspace, since the range of motion of the outer arms is restricted. This is represented by the unshaded area at the top of Fig. 7.

The unshaded (unreachable) region in Fig. 7 consists of two sectors with a triangular overlap, and its area may be calculated as:

$$\text{Unreachable Area}=\frac{1}{2}L_1^2(\phi+\delta)-[(Y_R-Y_{TP})\|Z_R\|] \tag{17}$$
$$\tan\phi=\frac{\|Z_R\|}{(Y_R-Y_{TP})+Y_A} \quad \tan\delta=\frac{\|Z_R\|}{(Y_R-Y_{TP})-Y_A}$$

Where $\|Z_R\|$ equals the absolute value of Z_R. The area of this unreachable region may then be subtracted from the result of applying the methods of Section 2.4.1 with the negative value of Z_R, yielding the reduced workspace cross sectional area. Note that this method may only be applied when rail two lies within the triangle formed by rail one, rail three and the lowest point of the workspace cross section.

3 Kinematic Optimization

It is the aim of this section to develop and solve the multi-dimensional, non-linear optimization problem of selecting geometric design variables for the Linear Delta that provide an acceptable compromise between manipulability and space utilization. The optimization considers the effect of the design variables on a utility function containing two performance indices, each calculated by analyzing an arbitrary cross section of the workspace. A numerical optimization has been carried out in the MATLAB environment, the formulation and results of which are presented in the following sections.

3.1 Design Variables. In order to reduce the number of variables and render the results independent of the scale of each design candidate, several non-dimensional ratios have been chosen as the design variables. These variables, shown in Table 1, have been selected to reflect intuitive measures of the relative proportions of the Linear Delta robot.

3.2 Performance Indices

3.2.1 Manipulability. The condition number of the Jacobian matrix, κ_J, has been used extensively in the literature to quantify the kinematic properties of manipulators [1,12,14,17,18]. The first performance index, η_1, measures the average value of $1/\kappa_J$ over the workspace cross section, normalized by the cross sectional area, A_W:

$$\eta_1 = \frac{\int_{A_W} \frac{1}{K_J} dA_W}{\int_{A_W} dA_W} = \frac{\int_{A_W} \frac{1}{K_J} dA_W}{A_W} \tag{18}$$

Adapted from [14], this index possesses several favorable characteristics. The index is normalized by the workspace size, and therefore gives a measure of kinematic performance independent of the differing workspace sizes of design candidates. Furthermore, the reciprocal of κ_J is bounded between 0 and 1, and is more convenient to handle than κ_J, which tends to infinity at singularities; hence, during numerical integration, the number of sample points near singularities has a reduced effect on the result since $1/\kappa_J$ approaches zero (rather than infinity) at these points. Lastly, the (dimensionless) value of the index lies between zero, for a manipulator singular in all configurations, and unity, for a manipulator perfectly kinematically isotropic in all configurations.

3.2.2 Space Utilization. This performance index was developed in order to overcome the problems involved in applying simple performance indices, in isolation, to the Linear Delta. For example, attempts to optimize the structure by maximizing η_1 alone led to an architecture with a large structural space requirement but a vanishing workspace size, due to the tending of L_2/L_1 towards zero; while the maximization of workspace cross sectional area caused the actuators to be collinear (i.e. $Y_R = 0$, since area increases monotonically with decreasing Y_R) resulting in a manipulator which is singular in all configurations. It became clear that a practical optimization of the Linear Delta would require a utility function comprising multiple performance indices.

Table 1 Kinematic design variables

Variable	Description	Restrictions
$\frac{L_1}{Y_R}$	Ratio of outer arm length to actuator separation.	$\geqslant 1$
$\frac{Y_A}{Y_R}$	Ratio of center actuator horizontal eccentricity to actuator separation.	0–1
$\frac{Z_R}{Y_R}$	Ratio of center actuator vertical eccentricity to actuator separation.	
$\frac{L_2}{L_1}$	Ratio of center arm length to outer arm length.	$\geqslant 0$

The space utilization performance index is defined as:

$$\eta_2 = \frac{\text{Workspace Cross Sectional Area}}{\text{Bounding Box Area}} = \frac{A_W}{\text{Bounding Box Area}} \tag{19}$$

where the bounding box is defined as the smallest rectangle in the *y-z* plane (the workspace cross section, such as that in Fig. 6), whose sides are parallel to the *y* and *z* axes, containing all three actuators and every point within the workspace cross section. The space utilization value reflects the ratio of workspace size to the physical size of the robot's structure. The index is dimensionless, bounded by the range [0 1], its calculation is simple and inexpensive (c.f. numerical integration of the Jacobian's condition number), and its value is independent of the overall scale of each design that it is applied to. Most importantly, designs requiring large volumes of space but yielding small workspaces are penalized.

The utility function for maximization is therefore defined as:

$$\eta = w_1 \left(\frac{\int_{A_W} \frac{1}{\kappa_J} dA_W}{A_W} \right) + w_2 \left(\frac{A_W}{\text{Bounding Box Area}} \right) = w_1 \eta_1 + w_2 \eta_2 \tag{20}$$

where w_1 and w_2 are positive weighting factors that define the relative importance placed on each performance index by the designer. The function is bounded by the range $[0 (w_1 + w_2)]$, and is independent of both the overall scale of the design candidate to which it is applied, and the limits chosen for the design variables (since neither performance index is normalized by its maximum observed value).

3.2.3 Computational Issues. An exhaustive (brute force) search method has been utilized to solve the optimization problem. While computationally expensive, an exhaustive search is simple, reduces the probability of any local maxima being overlooked, and provides information regarding the behavior of the utility function over the entire range of allowable values for each of the design variables.

The limits selected for the design variables are as follows: $1.4 \leqslant L_1/Y_R \leqslant 2.7$; $0 \leqslant Y_A/Y_R \leqslant 0.7$; $-0.5 \leqslant Z_R/Y_R \leqslant 0.5$; $0.6 \leqslant L_2/L_1 \leqslant .1.8$. Several of these limits are necessary to ensure that the resulting structure is practical. The remaining limits were chosen heuristically, with alterations made on a trial-and-error basis to yield a reasonably large range, and to ensure the inclusion of any local maxima of the utility function. A notable exception is the case where the manipulability index, η_1, was considered in isolation (i.e. $w_2 = 0$); in this situation L_2/L_1 was allowed to approach zero.

Since there exists no analytical means of calculating the Jacobian's condition number (κ_J), and therefore no closed-form expression for the manipulability index, numerical integration is required to determine the value of the utility function. The integral of Eq. (18) may be approximated by a discrete sum:

$$\eta_1 = \frac{\int_{A_W} \frac{1}{\kappa_J} dA_W}{A_W} \approx \frac{\sum_{a \in A_W} \frac{1}{\kappa_J}}{N_a} \tag{21}$$

where each a is one of N_a integration points in the *y-z* plane workspace cross section. These points are generated by examining the boundaries of the cross section and forming a uniformly distributed grid inside it.

In the majority of cases (such as that illustrated in Fig. 6), the closed form methods such as those shown in Sections 2.4.1 and 2.4.2 may be utilized to calculate the exact cross sectional area of

Table 2 Optimization results

Weights	Description	$\left(\frac{L_1}{Y_R}, \frac{Y_A}{Y_R}, \frac{Z_R}{Y_R}, \frac{L_2}{L_1}\right)$
$w_1=1,\ w_2=0$	Manipulability alone.	(1.55, 0, −0.75, →0)
$w_1=1,\ w_2=0$	Manipulability alone, with $Z_R=0$.	(1.48, 0, 0, 0.56)
$w_1=0,\ w_2=1$	Space utilization alone.	(2.00, 0, 0, 0.60)
$w_1=1,\ w_2=1$	Equally weighted utility function.	(2.00, 0, 0, 0.63)

the workspace (A_W). In some instances, however, the choice of design variables precludes the application of the closed form solutions, and it is necessary to approximate A_W. The following approximation has been utilized:

$$A_W \approx dA_W \cdot N_a \tag{22}$$

where dA_W is the small area associated with each of the N_a integration points. The accuracy of the approximation in (22) increases as N_a increases. Application of this equation to several situations in which a closed form solution for A_W existed revealed that if dA_W was sufficiently small such that $N_a > 5000$, then the relative error in A_W for these cases was generally less than 0.1%.

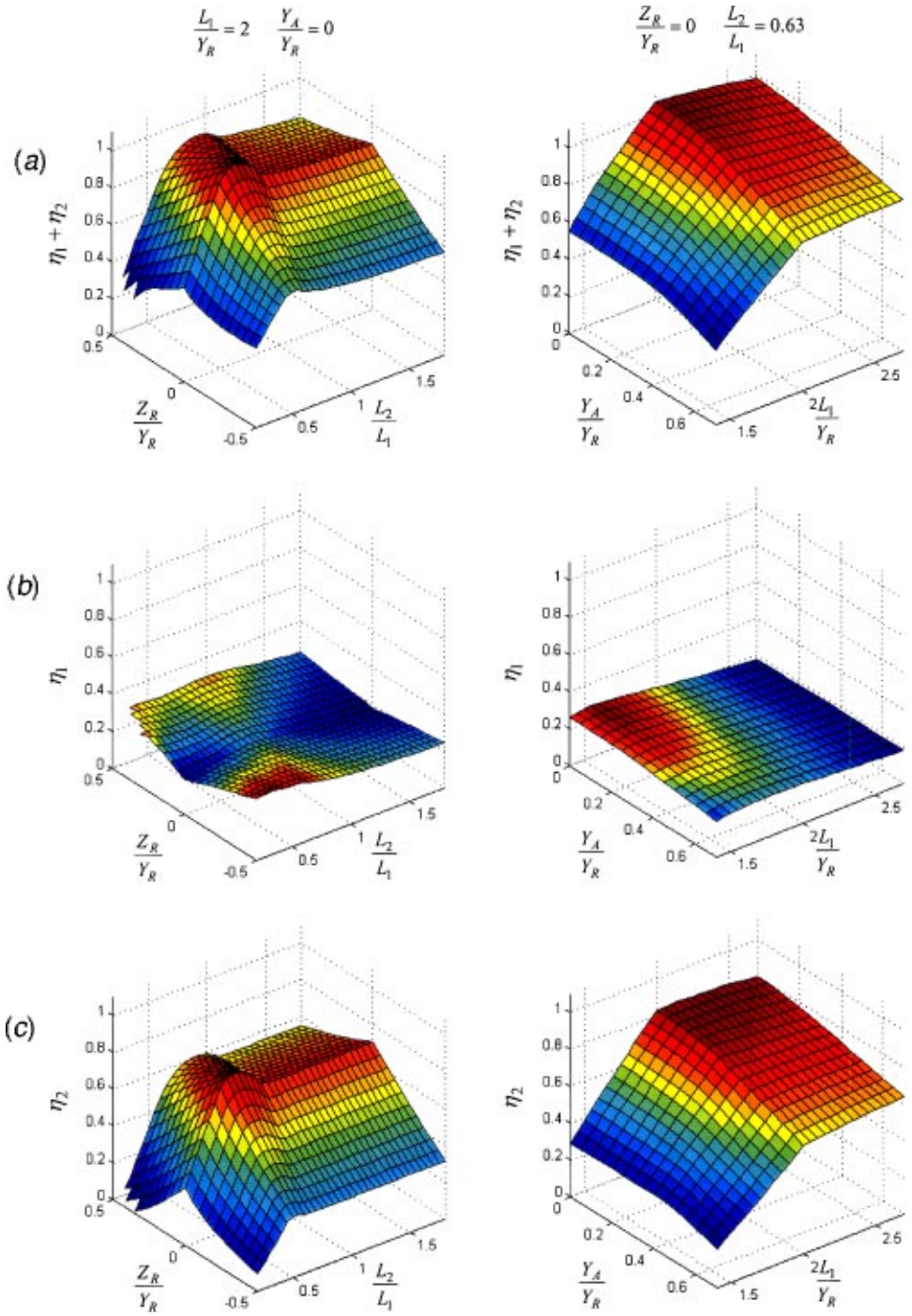

Fig. 8 Optimization results

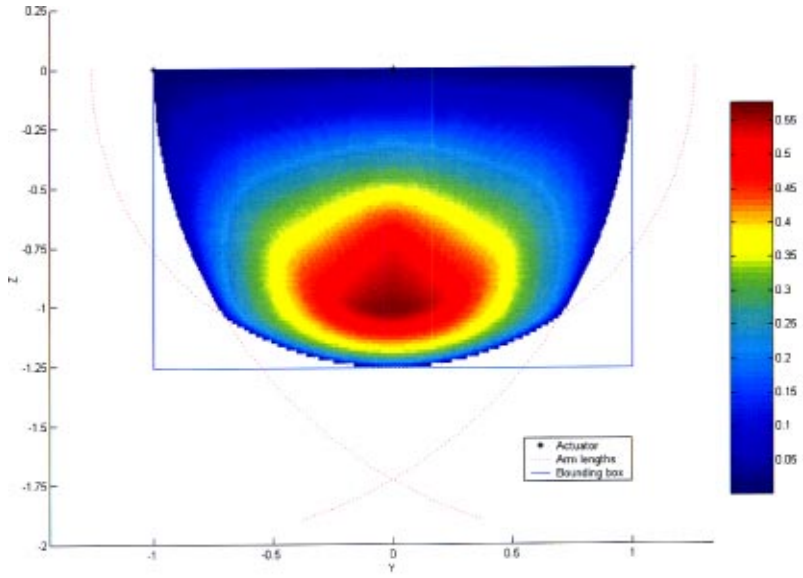

Fig. 9 Workspace cross section of optimal design, with colors showing value of $1/\kappa_J$

The complete four-dimensional optimization required approximately three hours of computation time using a Pentium II 200 MHz PC.

4 Results

Since the weights of the utility function, w_1 and w_2 in Eq. (20), are necessarily subjective, results for several combinations of values are presented in Table 2.

These values are correct to two decimal places. Visualization via several surface plots greatly aids the interpretation of these results. In Fig. 8, the values of (a) $\eta = \eta_1 + \eta_2$, (b) η_1, and (c) η_2 are shown. In order to present the four dimensional data set, two planes are displayed—each of which passes through the optimum point emboldened in Table 2. The shape of the workspace cross section for this optimal design is shown in Fig. 9.

The tendency for the solution to converge on a zero workspace size architecture when manipulability was optimized alone was the reason for developing the second performance index, space utilization. Other behaviors of the manipulability index that were noted include the confirmation that optimal value of Y_R is zero (a symmetrical architecture), and that for an arbitrary cross section through the four dimensional data set, manipulability generally exhibits relatively little variation when compared to space utilization.

The peaks and troughs shown in the space utilization surfaces may be explained intuitively by considering the effects of changes in the design variables to the workspace cross section. For example, the peak in space utilization at $L_1/Y_R = 2$ corresponds to architectures where the lengths of the outer arms are equal to the separation of the outer actuators—the width of the bounding box is then simultaneously determined by both the workspace and the structure. Reducing the ratio of outer arm length to actuator separation dramatically reduces η_2, since the workspace size falls without an accompanying reduction in the width of the bounding box. Increasing the ratio leads to modest reductions in space utilization, as the increasing size of the bounding box is partially offset by the expanding workspace area.

The optimum architecture is relatively insensitive to increasing w_1—large increases in the weighting of manipulability ($w_1 > 3$) are necessary before a considerable change in geometry is noted. While small increases in w_2 affect the results of the optimization, the change is limited to the variable L_2/L_1, with the greatest possible variation being a decrease of just 0.03.

5 Conclusions and Discussion

A method of multidimensional kinematic optimization of the parallel robot architecture's geometry was developed. A utility function, incorporating two performance indices, was formulated in order to determine those architectures which yield an optimum compromise between manipulability and a new performance index, space utilization. Space utilization is a concept designed to overcome the problems of small, non-singular workspaces often encountered when a parallel manipulator is optimized with only manipulability in mind. The exhaustive search algorithm was used to reliably find all prospective design candidates in four-dimensional parameter space. The method was shown to work extremely well and, therefore, is a viable competitor to advanced non-linear programming methods.

The proposed optimal design method was applied to the Linear Delta manipulator. A comprehensive study of the Linear Delta robot, a three translatory degree of freedom parallel manipulator, was conducted. Closed form solutions have been found for the forward and inverse kinematics and the Jacobian matrix.

The results presented here, and the suite of MATLAB programs created to perform the optimization, form a framework which may be utilized to create and analyze designs that result from selecting weighting factors that are appropriate to a specific application.

Acknowledgments

The financial support of The Australian Research council is gratefully acknowledged.

References

[1] Clavel, R., 1988, "DELTA, A Fast Robot with Parallel Geometry," *Proceedings of the 18th International Symposium on Industrial Robots, Lausanne (Switzerland), 26–28 April 1988*, C. W. Burckhardt, ed., International Federation of Robotics, IFS Publications, UK, pp. 91–97.

[2] Clavel, R., 1991, "Conception d'un robot parallele rapide a 4 degres de liberte," PhD Thesis No. 925. Swiss Federal Institute of Technology (EPFL), Lausanne.

[3] Herve, J. M., 1994, "Methodological Design of New Parallel Robots via the

Lie Group of Displacements,'' *Proc. of CISM/IFToMM Conference Ro.Man.Sy. '94*, Gdansk, pp. 301–306.
[4] Merlet, J. P., 1990, *Les Robots Paralleles*, Hermes, Paris.
[5] Miller, K., 2001, ''Maximization of Workspace Volume of 3-dof Spatial Parallel Manipulators,'' ASME J. Mech. Des., **124**(2), pp. 347–350.
[6] Pierrot, F., Dauchez, P., and Fournier, A., 1991, ''Hexa, a Fast 6-Degree of Freedom Fully Parallel Robot,'' *Proc. of International Conference on Advanced Robotics*, Pisa, Vol. 2/2, pp. 1158–1163.
[7] Stewart, D., 1966, ''A Platform With Six Degrees of Freedom,'' Proc. Inst. Mech. Eng., **180**(I), No. 15, pp. 371–386.
[8] Tsai, L. W., 1999, *Robot Analysis: The Mechanics of Serial and Parallel Manipulators*, John Wiley & Sons, New York, N.Y.
[9] Miller, K., and Clavel, R., 1992, ''The Lagrange-based Model of Delta-4 Robot Dynamics,'' *Robotersysteme 8*, Springer-Verlag, pp. 49–54.
[10] Merlet, J.-P., 1993, ''Direct Kinematics of parallel manipulators,'' IEEE Trans. Rob. Autom., **9**(6), pp. 842–846.
[11] Carretero, J. A., Nahon, M., and Podhorodeski, R. P., 1998, ''Workspace Analysis of a 3-dof Parallel Mechanism,'' *Proceedings of the 1998 IEEE/RSJ International Conference on Intelligent Robots and Systems*, IEEE Piscataway, NJ, Vol. 2, pp. 1021–1026.
[12] Stamper, R. E., Tsai, L.-W., and Walsh, G. C., 1997, ''Optimization of a Three DOF Translational Platform for Well-Conditioned Workspace,'' *Proceedings of the 1997 IEEE International Conference on Robotics and Automation*, IEEE Piscataway, NJ, Vol. 4 pp. 3250–3255.
[13] Wang, L.-C. T., and Hsieh, J.-H., 1998, ''Extreme Reaches and Reachable Workspace Analysis of General Parallel Robotic Manipulators,'' J. Rob. Syst., **15**(3), pp. 145–159.
[14] Gosselin, C., and Angeles, J., 1989, ''The Optimum Kinematic Design of a Spherical Three-Degree-of-Freedom Parallel Manipulator,'' ASME J. Mech. Trans., Autom. Des. **111**(2), pp. 202–207.
[15] Tsai, L.-W., Walsh, G. C., and Stamper, R. E., 1996, ''Kinematics of a Novel Three DOF Translation Platform,'' *Proceedings of the 1996 IEEE 13th International Conference on Robotics and Automation*, IEEE Piscataway, NJ, Vol. 4, pp. 3446–3451.
[16] Merlet, J.-P., 1992, ''On the Infinitesimal Motion of Parallel Manipulators in Singular Configurations,'' *Proceedings of the 1992 IEEE International Conference on Robotics and Automation*, IEEE Piscataway, NJ, Vol. 1, pp. 320–325.
[17] Gosselin, C., and Angeles, J., 1988, ''The Optimum Kinematic Design of a Planar Three-Degree-of-Freedom Parallel Manipulator,'' ASME J. Mech., Trans., Autom. Des., **110**(1), pp. 35–41.
[18] Kurtz, R., and Hayward, V., 1992, ''Multiple-goal Kinematic Optimization of a Parallel Spherical Mechanism with Actuator Redundancy,'' IEEE Trans. Rob. Autom., **8**(5), pp. 644–651.